AGU PUBLICATIONS

JGR

Journal of Geophysical Research: Biogeosciences

RESEARCH ARTICLE
10.1002/2014JG002870

**Key Points:**
- Temporal and spatial variability in hydrodynamics is key to marsh establishment
- Tidal flat morphology determines marsh vegetation establishment patterns
- Applying "windows of opportunity" concept can assist marsh restoration

**Correspondence to:**
Z. Hu,
zhan.hu@nioz.nl

**Citation:**
Hu, Z., J. van Belzen, D. van der Wal, T. Balke, Z. B. Wang, M. Stive, and T. J. Bouma (2015), Windows of opportunity for salt marsh vegetation establishment on bare tidal flats: The importance of temporal and spatial variability in hydrodynamic forcing, *J. Geophys. Res. Biogeosci.*, *120*, 1450–1469, doi:10.1002/2014JG002870.

Received 25 NOV 2014
Accepted 2 JUL 2015
Accepted article online 14 JUL 2015
Published online 31 JUL 2015



# Windows of opportunity for salt marsh vegetation establishment on bare tidal flats: The importance of temporal and spatial variability in hydrodynamic forcing

**Zhan Hu[1,2], Jim van Belzen[1], Daphne van der Wal[1], Thorsten Balke[1,3], Zheng Bing Wang[2,4], Marcel Stive[2], and Tjeerd J. Bouma[1]**

[1]Spatial Ecology Department, Royal Netherlands Institute for Sea Research, Yerseke, Netherlands, [2]Hydraulic Engineering Department, Delft University of Technology, Delft, Netherlands, [3]Institute for Biology and Environmental Science, Carl von Ossietzky University Oldenburg, Oldenburg, Germany, [4]Deltares, Delft, Netherlands

**Abstract** Understanding the mechanisms limiting and facilitating salt marsh vegetation initial establishment is of widespread importance due to the many valuable services salt marsh ecosystems offer. Salt marsh dynamics have been investigated by many previous studies, but the mechanisms that enable or disable salt marsh initial establishment are still understudied. Recently, the "windows of opportunity" (WoO) concept has been proposed as a framework providing an explanation for the initial establishment of biogeomorphic ecosystems and the role of physical disturbance herein. A WoO is a sufficiently long disturbance-free period following seedling dispersal, which enables successful establishment. By quantifying the occurrence of WoO, vegetation establishment pattern can be predicted. For simplicity sake and as prove of concept, the original WoO framework considers tidal inundation as the only physical disturbance to salt marsh establishment, whereas the known disturbance from tidal currents and wind waves is ignored. In this study, we incorporate hydrodynamic forcing in the WoO framework. Its spatial and temporal variability is considered explicitly in a salt marsh establishment model. We used this model to explain the observed episodic salt marsh recruitment in the Westerschelde Estuary, Netherlands. Our results reveal that this model can significantly increase the spatial prediction accuracy of salt marsh establishment compared to a model that excludes the hydrodynamic disturbance. Using the better performing model, we further illustrate how tidal flat morphology determines salt marsh establishing elevation and width via hydrodynamic force distribution. Our model thus offers a valuable tool to understand and predict bottlenecks of salt marsh restoration and consequences of changing environmental conditions due to climate change.

## 1. Introduction

Although the question if salt marshes may keep pace with sea level rise by sediment accretion has gained a lot of attention [e.g., *Allen*, 1995; *Reed*, 1995; *Cahoon et al.*, 2006; *Kirwan et al.*, 2010; *Kirwan and Megonigal*, 2013], understanding of the mechanisms affecting lateral expansion and retreat of salt marshes, such as plants recruitment and cliff erosion, is still limited [*van de Koppel et al.*, 2005; *Mariotti and Fagherazzi*, 2010]. Especially, processes that enable or disable the initial establishment of salt marsh vegetation on bare tidal flats are still poorly studied [*Balke et al.*, 2014]. Hence, mechanistic insight into these processes is essential for the effective management and restoration of salt marshes worldwide [*Viles et al.*, 2008; *Spencer and Harvey*, 2012].

Salt marsh plant recruitment on bare tidal flats often occurs during episodic events as consequences of interactions between ecological, physical, and biogeochemical processes [*Balke et al.*, 2014]. Typically, the suitable elevation for salt marsh establishment is described as an empirically derived minimum elevation [e.g., *McKee and Patrick*, 1988; *Morris et al.*, 2002; *Wang and Temmerman*, 2013] mainly arguing with physiological limits of salt marsh plants to inundation stress. *Wang and Temmerman* [2013] have described in a remote sensing study for the Westerschelde Estuary that a minimum elevation of −0.5 m to −0.6 m above local MHWL (mean high water level) is suitable for colonization. Yet such empirical descriptions do not provide insights into the key mechanisms determining colonization of tidal flats [*Spencer and Harvey*, 2012; *Balke et al.*, 2014]. Without appreciation of the responsible processes, the empirically derived approach for

vegetation establishment prediction is limited to the specific environment it is applied to. In cases of changing location or external condition, the prediction becomes less reliable. For instance, a large variation in the elevation of the seaward pioneer vegetation edge is observed across different salt marshes in the Westerschelde Estuary [*van der Wal et al*., 2008], which may not be explained by a single empirical relation.

Recently, *Balke et al*. [2014] suggested that disturbance-free periods of a defined minimum duration, called "windows of opportunity" (WoO), can be identified from time series analysis to hindcast and potentially predict colonization events in ecosystems where new establishment is disturbance limited. Examples in dunes, floodplains, mangroves, and salt marshes suggested that wind and water movement is needed to disperse the diaspores to vacant bare areas for colonization [*Balke et al*., 2014]. And yet the same processes also can inhibit seedling establishment as they form strong physical disturbance in these bare areas [*Balke et al*., 2014]. Therefore, the temporal variability of, e.g., hydrodynamic forcing from tidal current and wind waves is essential for enabling the salt marsh colonization of new areas while it may also form the bottleneck to seedling survival after the dispersal. Since the WoO concept provides mechanistic insight, it may become a widely applicable predictive tool for new establishment in coastal marshes and other disturbance-limited ecosystems, once the underlying mechanisms can be correctly reproduced in a modeling approach.

Using a simple tidal level time series analysis for inundation-free period following a high tide that dispersed the seeds, it was possible to identify a salt marsh recruitment event on a bare tidal flat [*Balke et al*., 2014]. This analysis, however, did not account for hydrodynamic stresses that originate from waves and currents. Physical disturbance induced by hydrodynamics (i.e., waves and currents) and associated sediment dynamics (i.e., erosion and deposition at the bed) is known to potentially be the main bottleneck to seedling establishment on tidal flats fronting salt marshes [*Temmerman et al*., 2007; *Bouma et al*., 2009; *Schwarz et al*., 2011; *Friess et al*., 2012; *Spencer and Harvey*, 2012] and mangroves [*Balke et al*., 2011, 2013]. In order to develop the WoO approach into a powerful predictive tool, it is hence necessary to expand the time series analysis from a solely disturbance frequency-driven analysis that only accounts for water level fluctuations, to a spatially explicit disturbance frequency-driven and disturbance magnitude-driven analysis that accounts for both water level fluctuations and gradients of hydrodynamic forcing.

Hydrodynamic forcing causes seedling failure by directly imposing drag on the propagule or seedling or by suspending/eroding the bed sediment and hence excavating the seedling. For mangrove seedlings, both mechanisms are critical to their establishment as large propagules can directly be pulled out of the bed [*Balke et al*., 2011]. For salt marsh seedlings, however, the size of the seedlings in the first days after germination (i.e., the frontal area facing drag force) is much smaller compared to the rooted mangrove propagule [*Friess et al*., 2012]. Therefore, the direct drag on marsh seedlings in the first days after germination is limited, and the sediment resuspension/erosion is expected to be the main mechanism causing salt marsh seedling failures. A relevant proxy for the sediment resuspension is bed shear stress (BSS) induced by waves and currents [e.g., *Fagherazzi et al*., 2006; *Green and Coco*, 2007; *Carniello et al*., 2005, 2011; *Callaghan et al*., 2010]. Young seedlings will be exposed to BSS disturbance upon flooding, regardless of their root anchorage depth. They will be dislodged from tidal flats, if the seedling roots have not grown into a sufficient depth (e.g., a few centimeters) to withstand the BSS and associated sediment resuspension/erosion. Therefore, it is important to incorporate the BSS disturbance and seedling root growth in the prediction of the salt marsh establishment.

In the present study, we hypothesize that successful seedling establishment on bare tidal flats requires a first WoO consisting of a sufficiently long inundation-free period (e.g., 3 days) for germination and initial root anchorage against flooding (i.e., WoO1), as proposed by *Balke et al*. [2014]. This WoO1 needs to be followed by a second WoO (i.e., WoO2, for 2–4 weeks), in which time-dependent BSS needs to remain below a critical value determined by seedling age and hence seedling root length. Disturbance frequency and disturbance magnitude are thus considered in WoO1 and WoO2, respectively.

The spatial distribution of BSS over a tidal flat is typically influenced by its bathymetry and hydrodynamic conditions, including, e.g., tidal level, wind velocity, and fetch [e.g., *Le Hir et al*., 2000; *Fagherazzi et al*., 2006; *Marani et al*., 2007; *Mariotti and Fagherazzi*, 2013; *Green and Coco*, 2014]. We therefore hypothesize that the newly established seedlings may experience different magnitude of disturbance on different tidal flat profiles, even if the encountered hydrodynamic boundary conditions are similar. Thus, the morphology

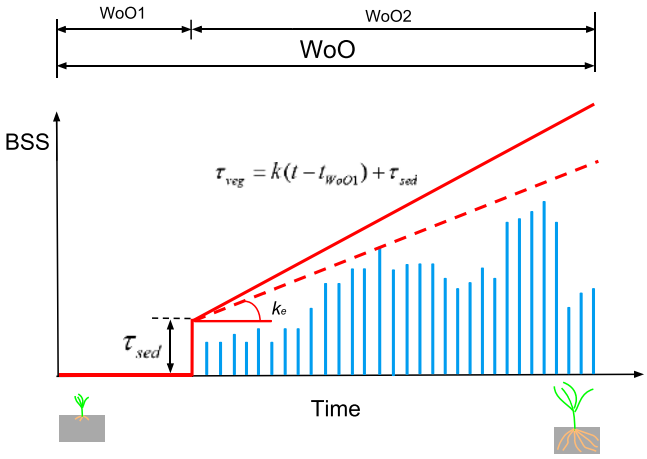


**Figure 1.** Schematization of the perdition based on WoO1&WoO2; WoO1 is an inundation-free period with a critical minimum duration (BSS is zero); WoO2 is a period following WoO1, when the seedlings are experiencing BSS disturbance (the blue line). If during WoO2 the external BSS stays lower than the $\tau_{veg}$ (red solid line), then WoO events occur for seedling establishment. $\tau_{veg}$ increases with seedling age because of seedlings roots development, whose increase rate is $k$. The red dashed line indicates $k_e$ as the maximum slope derived from the BSS time series, which incorporates both magnitude and timing of the external forcing (equation (2)). By comparing $k_e$ and external $k$, we can determine if the disturbance magnitude exceeds the threshold for seedlings survivals in the WoO2.

of a tidal flat may play a key role in providing abiotic conditions for marsh plant establishment and may be equally important than the elevation zone and inundation period itself. Tidal flats typically have a contrasting convex or concave shape and different profile slopes [*Friedrichs*, 2011; *Bearman et al*., 2010]. On different tidal flat profiles, the abiotic conditions for plant establishment can be assessed by the lowest elevation for plant establishment (LE). The profiles that have lower LE for a certain pioneer salt marsh species are the ones that provide more favorable abiotic condition for seedling establishment, which ultimately leads to larger overall salt marsh areas. Thus, the variation in tidal flat bathymetry may affect the outcomes of salt marsh conservation and restoration efforts.

The objectives of our study are twofold. First, we wanted to test the importance of including the disturbance magnitude (hydrodynamic forcing)-related WoO2 in our ability to predict seedling establishment. Hence, we build two vegetation establishment models with or without considering the WoO2, i.e., WoO1 model versus a WoO1&WoO2 model. These two models were quantitatively compared for their ability to explain observed vegetation establishment patterns on a tidal flat in the Westerschelde Estuary, Netherlands. The spatial-temporal dynamics of BSS at the study site was provided by hydrodynamic modeling, which has been validated against field measurements. Second, we aimed to gain insights in the effect of tidal flat morphology on seedling establishment. Hence, we predicted vegetation establishment patterns on schematized tidal flat profiles using a calibrated WoO model. Convex- and concave-shaped tidal flats with different slopes were tested to find the lowest tidal elevation threshold for plants establishment (LE) and associated salt marsh width. The results of LE and salt marsh width on different profiles are discussed for their importance to restoration and management of salt marshes.

## 2. Method

### 2.1. Alternative Models for Vegetation Establishment Based on WoO

To understand initial seedling establishment patterns and test the importance of including hydrodynamic forcing, two analytical salt marsh establishment models were built. One model solely considers a long enough inundation-free period following a (seed-dispersing) high tide as a windows of opportunity (WoO) for seedling establishment, which will be referred to as the WoO1 model. The other model considers an additional subsequent period (WoO2) when the seedlings are exposed to BSS, i.e., the WoO1&WoO2 model (Figure 1). Both models consider seedling survival rather than seed availability as the bottleneck for salt marsh establishment [*Balke et al*., 2014; *Temmerman et al*., 2007; *Zhu et al*., 2014].

For the WoO1 model, long inundation-free periods typically occur when the daily high tidal level is declining (i.e., from spring to neap tide). In this phase of the spring-neap tidal cycle, receding water can deliver diaspores to a sufficient high elevation, where inundation disturbance is absent in the following period. For a certain elevation, inundation-free periods can be identified by analyzing time series of the tidal water level. If such an inundation-free period is sufficiently long, then it is regarded as a WoO1 that may enable seedling establishment. The required minimum inundation-free period is $t_{WoO1}$, which is the only calibration parameter in the WoO1 model.

The situation that seedling establishment requires both WoO1&WoO2 is schematized in Figure 1. The WoO1&WoO2 model does not quantify the sediment transport process but quantifies the BSS as a proxy of the bed sediment disturbance. As WoO1 is an inundation-free period, BSS is by definition absent (zero). WoO2 is the period following WoO1, when the seedlings are inundated and become exposed to BSS. Its duration is $t_{WoO2}$. The WoO2 is characterized by the critical BSS for seedlings survival (, $\tau_{veg}$), which describes the plant tolerance to hydrodynamic forcing. If BSS stays below the corresponding $\tau_{veg}$ during the WoO2, then seedlings will become successfully established (Figure 1). If the BSS exceeds $\tau_{veg}$ at any moment in WoO2, then seedlings cannot be successfully established due to the prohibitive disturbance. At the initial growing stage of the seedlings, we assume that $\tau_{veg}$ increases linearly with time following dispersal due to seedling root development [*Balke et al.*, 2011]. $\tau_{veg}$ is greater than the critical BSS for sediment motion initiation ($\tau_{sed}$), as the forcing needs to be at least strong enough to mobilize bed sediment in order to dislodge rooted seedlings. Thus, the $\tau_{veg}$ function starts at the point ($t_{WoO1}$, $\tau_{sed}$) and increase linearly over time:

$$\tau_{veg} = k(t - t_{WoO1}) + \tau_{sed} \tag{1}$$

where $t$ is the age of the seedlings after dispersal in hours and $k$ is the growth rate of the $\tau_{veg}$ in Pa/h. $k$ is related to seedlings root growth, which may be influenced by plants species, temperature, salinity, substrate type, and moisture [*Mudd et al.*, 2009; *Kirwan and Guntenspergen*, 2012; *Booth and Loheide*, 2012]. In this study, $k$ is a calibration parameter, as for salt marsh plants, the estimates of $k$ have not yet been reported in the literature. Alternatively, based on a flume experiment using mangrove seedlings, a $k$ value can be estimated to be $3.3 \times 10^{-3}$ Pa/h [*Balke et al.*, 2011]. Due to the uncertainty that lays in the $k$ value, a sensitivity analysis was carried out by varying $k$ in a wide range to assess model robustness and explore its effect on the modeled vegetation establishment pattern.

In order to describe the external BSS forcing conditions in relation to the seedlings development, a slope of BSS can be derived for each time step in WoO2 to incorporate both instantaneous BSS magnitude and its timing. The maximum slope in WoO2 is selected to be the characteristic value ($k_e$) representing the overall external forcing (Figure 1):

$$k_e = \left(\frac{\mathrm{BSS}(t) - \tau_{sed}}{t - t_{WoO1}}\right) \tag{2}$$

$k_e$ can be regarded as the required growth rate of a seedling BSS tolerance to the external conditions. Therefore, the comparison between BSS and $\tau_{veg}$ can be assessed by comparing $k_e$ and $k$. If $k_e > k$, the external BSS will then exceed the corresponding $\tau_{veg}$ at a certain time step in WoO2. Thus, the external forcing is too severe for seedlings survival. If $k_e \leq k$, the BSS stays below $\tau_{veg}$ during the whole WoO2; i.e., the external forcing is mild and suitable for seedling establishment (Figure 1). BSS time series are provided by hydrodynamic simulations including both wind waves and tidal currents, which are described in section 2.3.

For both vegetation establishment models, salt marsh establishment pattern can be predicted by quantifying the WoO occurrence during the growing season (e.g., 1 April to 1 October) [*Balke et al.*, 2014]. For a tidal flat transect, prediction can be made for each 1 m segment. If a segment has one or more WoO occurrences, then it is predicted to become colonized [*Balke et al.*, 2014] and it is assigned a value of "1." If a segment does not have any WoO, it is predicted to stay bare and is assigned a value of "0." Similar 1/0 distribution treatment will be applied in the vegetation establishment observations to facilitate the model performance evaluation.

### 2.2. Observations of Vegetation Establishment

To test the two alternative vegetation establishment models, we used observations of vegetation dynamics on a tidal flat (Zuidgors, near Ellewoutsdijk) in the Westerschelde Estuary, SW Netherlands (Figure 2). The Westerschelde is a mesotidal to macrotidal estuary. At the study site, the mean tide range and mean high water level (MHWL) is 4.1 m and 2.3 m NAP (Normal Amsterdam Peil), respectively [*Callaghan et al.*, 2010]. The bare tidal flat in front of the mature salt marsh is exposed to air at low tide and submerged at high tide with water depth being 1 m to 3 m. On the mature salt marsh, the water depth can vary from 0 to 0.6 m. As the tidal flat is on the northern bank of the Westerschelde, it is exposed to the prevailing southwesterly winds. It leads to higher incident waves compared to the tidal flats on the southern bank

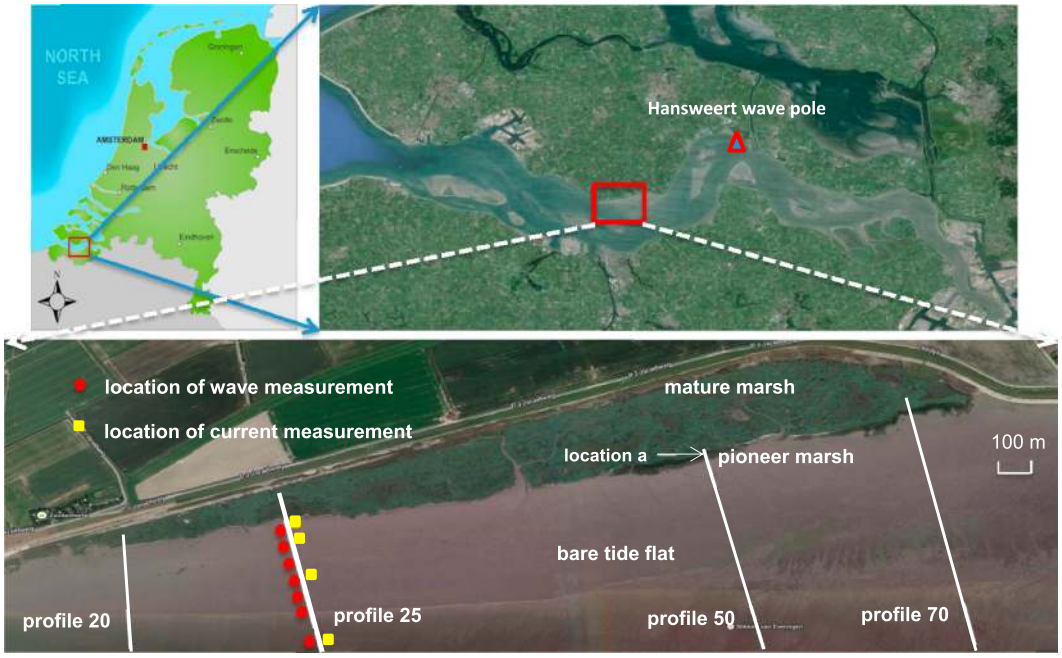


**Figure 2.** Study site near Ellewoutsdijk in the Westerschelde Estuary, SW of Netherlands. Profiles 20, 25, 50, and 70 are monitored for vegetation establishment. Hydrodynamic measurements were carried out on profile 25. A nearby wave pole at Hansweert is indicated as a red triangle, which provides long-term wave data for BSS quantification. Time series of BSS at location *a* (1.85 m NAP) is shown as examples in the following section 3.2. Images are from Google Earth.

[*Callaghan et al*., 2010]. At the study site, $\tau_{sed}$ is estimated to be 0.15 Pa, which is close to estimation in *Callaghan et al*. [2010] (0.13 Pa) for the same tidal flat. The estimation is based on the average medium sediment grain diameter measured in March, May, and September 2006 ($d_{50} = 82$ μm) [*van Rijn*, 2007]. The effect of clay coating and biogenic cohesion on $\tau_{sed}$ was not accounted for due to a lack of detailed information on sediment fractions. In reality, $\tau_{sed}$ varies both in space and in time. For the sake of simplicity, it is assumed to be constant in this study.

The potential pioneer zone is in front of distinctive salt marsh cliffs. The pioneer vegetation on this tidal flat is predominately *Spartina anglica* with some *Salicornia* and *Aster tripolium* being the secondary species [*van der Wal et al*., 2008]. In this study, a single *k* value is assumed, as there is no sufficient data to distinguish between species. The potential pioneer zone was defined as the area from the mature salt marsh edge (i.e., cliff at approximately 2.2 m NAP) until 1.7 m NAP. The lower boundary of the potential pioneer zone was the elevation threshold suggested by *Wang and Temmerman* [2013] (−0.6 m to MHWL), above which plants have a high chance of establishment. It is noted that the lower boundary at 1.7 m NAP is different from the lowest elevation for plant establishment (LE). LE is the lowest elevation predict by the model, where vegetation colonization occurs, whereas the lower boundary suggested by *Wang and Temmerman* [2013] indicates a generic elevation limit based on empirical data, above which vegetation colonization may occur.

The areas that are lower than this potential pioneer zone (lower than 1.7 m NAP) would have very limited chance for establishment. It is expected that both WoO1 and WoO1&WoO2 models will give similar predictions for these lower areas, i.e., no establishment, which is not helpful for the comparison of the two models. Therefore, we confined vegetation recruitment modeling and the corresponding vegetation cover monitoring in the potential pioneer zone, where the two models are expected to give different predictions. Based on these different predictions and the observation in this zone, the performance of the two models can be assessed. Additionally, the position of the marsh cliff can move landward over time due to lateral erosion. The position change was adapted in the analysis.

Vegetation establishment patterns were obtained along four cross-shore profiles from west to east (profiles 20, 25, 50, and 70, Figure 2) based on aerial photographs. Each profile was divided into 1 m long segments. A segment was considered being successfully colonized by seedlings if it shifted from bare state to vegetated

state in two subsequent aerial images. Similar to the WoO models, segments that were colonized are assigned a value of 1, whereas those that stayed bare were assigned a value of 0. Vegetation absence and presence between 2001 and 2013 were classified based on normalized difference vegetation index from false-color aerial images provided by the Dutch Department of Public Works and Water Management. The aerial images of this area, generally taken on a 1:5000 scale, were taken in 2001, 2004, 2007, 2010, 2011, and 2012. To narrow down the period in which recruitment took place, we further used true-color images obtained from Google Earth from 2005 and 2013 as supplements. These images were classified based on the Green Excess Index [*Richardson et al.*, 2009].

Elevation (expressed in m NAP) of the intertidal zone from detailed ground leveling was available from the Dutch Department of Public Works and Water Management along profiles 20, 50, and 70 for 2004. In 2012, these elevation profiles were obtained from interpolation of data with 20 m resolution from a combination of airborne laser altimetry and shipborne single-beam/multibeam bathymetric surveys. The intertidal topography of profile 25 was measured by laser leveling and dGPS equipment in 2004 and 2012, respectively. To facilitate hydrodynamic modeling, profiles were extended downward till −1.62 m NAP if the original profiles did not reach this seaward boundary elevation, by extracting information from the 20 m resolution surveys in a geographical information system.

### 2.3. Hydrodynamic Measurements and Bed Shear Stress Quantification

#### 2.3.1. Wave and Tidal Current Measurement on Profile 25

The model including WoO2 requires the information of temporal and spatial BSS variations. This information was provided by means of hydrodynamic modeling. To obtain data for validating the hydrodynamic model, we measured tidal level, wind wave, and current velocity along profile 25 (Figure 2). Seven pressure sensors (Coastal Leasing, Inc.) were deployed in October and November 2012 to measure the water level and wave characteristics. They were placed 0.05 m above the seabed at the following elevations: −1.62 m NAP, −0.64 m NAP, 0.37 m NAP, 1.01 m NAP, 1.43 m NAP, 1.58 m NAP, and 1.74 m NAP. Measuring frequency was 4 Hz, and measuring interval was 15 min. A total of 4096 data points were obtained in each measuring interval. The water level is determined as the mean value measured in an interval. The recorded water level data were compared to the nearby tide gauge at Terneuzen in order to obtain water level data outside the validation period. The wave analysis was based on pressure fluctuations. The attenuation of the pressure signals with water depth was corrected to derive bulk wave parameters, e.g., significant wave height ($H_s$) and peak wave period ($T_P$) [*Tucker and Pitt*, 2001]. The measured significant wave height at the edge of the tidal flat ($H_s$ at −1.62 m NAP) was linked to the significant wave height ($H_{s\_pole}$) measured by a nearby wave pole at Hansweert (Figure 2) in the same measuring period. An empirical relation between the $H_s$ at −1.62 m NAP and the $H_{s\_pole}$ was derived as

$$H_s = 0.58 \times H_{s\_pole} - 0.01 \quad \left(R^2 = 0.62\right) \tag{3}$$

This relation was used to provide incident wave height for wave modeling and BSS quantification in the growing seasons of different years, when in situ wave data were not available. Tidal current velocity was measured using four acoustic Doppler current profilers (ADCPs) from December 2013 to January 2014. They were placed in the seabed at the following elevations: −1.56 m NAP, 1.06 m NAP, 1.70 m NAP, and 1.77 m NAP. The measuring interval was 10 min. We conducted harmonic analysis using measured depth-averaged current velocity at the most seaward ADCP and a package of MATLAB routines called T_TIDE [*Pawlowicz et al.*, 2002]. In total, 29 main tidal constituents were detected in the dominating longshore tidal current, which facilitates future tidal velocity predictions.

#### 2.3.2. Wave and Tidal Current Modeling

To be able to obtain BSS along the elevation gradient of the whole tidal flat, a hydrodynamic model was constructed to quantify wave height and tidal current velocity. Wind wave propagation on the tidal flats was simulated by a 1-D spectral model using Simulating Waves Nearshore [*Booij et al.*, 1999]. This model accounts explicitly for wave shoaling, breaking, and bed friction processes in varying external conditions. Wave modeling domains were created for each monitored tidal profile indicated in Figure 2. The elevation of the modeling domains was from −1.62 m NAP until the salt marsh cliff. The grid size of the computation domain is 1 m, which is the same as the WoO models to enable WoO quantifications. The model was forced by incident waves with a Joint North Sea Wave Project spectrum [*Hasselmann et al.*, 1973], while wind force was excluded. During the field measurement period, incident wave parameters ($H_s$ and peak period $T_p$) were

provided by the most seaward pressure sensor. Outside the field measurement period, $H_s$ data were provided by the long-term wave pole measurements via the empirical relation (3). In the growing seasons when the field observation is not available, $T_p$ was assumed to be the mean value of the field measurements ($T_p = 2.8$ s, standard deviation = 0.81 s) for simplicity sake. This assumption is reasonable, as the interested pioneer zone is mostly in shallow water condition based on measurements (i.e., 0.2 m −0.5 m water depth with $T_p$ longer than 2.0 s). In such a condition, the variation in $T_p$ does not have an apparent effect on BSS. Parameters that describe wave propagation processes were set as default values (see http://swanmodel.sourceforge.net/).

Tidal current velocity modeling shared the same computation domains and grid size as the wave model. Cross-shore and longshore tidal current velocity was modeled separately. The magnitude of the cross-shore current ($u_c$) was derived based on a water volume conservation [*Friedrichs and Aubrey*, 1996; *Le Hir et al*., 2000]. As the tide rises, the water line moves landward, which is attended by an onshore flow. The volume of water ($\Delta V$) that must pass through a vertical plane (at location $x$) parallel to the shore equals to the increase in the water volume of the area that is landward of location $x$. $\Delta V$ can be determined based on tidal flat bathymetry and the rise of the surface level assuming that it remains horizontal in every tidal phase. Then, the cross-shore current ($u_c(x)$) that infills this volume in a time interval $\Delta t$ is

$$u_c(x) = \frac{\Delta V(x)}{\Delta t h(x) B} \tag{4}$$

where $B$ is the unit alongshore width of the flat and $h(x)$ is the water depth at a certain location on the tidal flat. The alongshore tidal current at the seaward boundary ($u_{l\_\mathrm{out}}$ in m/s) was predicted by T_TIDE based on previously derived tidal constituents [*Pawlowicz et al*., 2002]. Subsequently, the alongshore tidal current velocity at location $x$ ($u_l(x)$) can be derived by considering balancing the bed friction and longshore water level gradient [*Le Hir et al*., 2000]. Such a gradient is assumed to be uniform on a tidal flat transect since the tide propagation often has a much larger scale than a cross section of a tidal flat. We further assume that bed friction is proportional to the square of the depth-averaged velocity [*Le Hir et al*., 2000]. The $u_l(x)$ is then determined as

$$u_l(x) = u_{l\_\mathrm{out}} \sqrt{\frac{h(x)}{h_{\mathrm{out}}}} \tag{5}$$

where $h_{\mathrm{out}}$ is the water depth at the seaward boundary. The total tidal current velocity is

$$u = \sqrt{u_c^2 + u_l^2} \tag{6}$$

The angle between the tidal current velocity and shore normal direction is

$$\theta = \tan^{-1}\left(\frac{u_l}{u_c}\right) \tag{7}$$

The hydrodynamic model performance is evaluated using the scatter index (SCI) and relative bias scores (Rel. bias) to compare the model output against in situ measurements, which are defined as

$$\mathrm{SCI} = \frac{\sqrt{\frac{1}{n}\sum_{i=1}^{n}\left(\Psi^i_{\mathrm{model}} - \Psi^i_{\mathrm{obs}}\right)^2}}{\frac{1}{n}\sum_{i=1}^{n}\Psi^i_{\mathrm{obs}}} \tag{8}$$

$$\mathrm{bias} = \sum_{i=1}^{n}\left(\Psi^i_{\mathrm{model}} - \Psi^i_{\mathrm{obs}}\right) \tag{9}$$

$$\mathrm{Rel.bias} = \frac{\sum_{i=1}^{n}\left(\Psi^i_{\mathrm{model}} - \Psi^i_{\mathrm{obs}}\right)}{\sum_{i=1}^{n}\Psi^i_{\mathrm{obs}}} \tag{10}$$

where $\Psi^i_{\mathrm{obs}}$ is the data from the observations; $\Psi^i_{\mathrm{model}}$ is the corresponding model output; and $n$ is the number of the total observations. SCI and Rel.bias give a comprehensive evaluation of the models. The closer SCI and Rel.bias values to zero indicate a better model performance. The hydrodynamic model performance was assessed based on two main parameters: $H_s$ and $u$ (Figure 3). The SCI and Rel.bias values of $H_s$ are 0.157 and −0.070 based on 12,860 data points, whereas the SCI and Rel.bias values of $u$ are 0.214 and −0.069 based on 16,128 data points. The SCI and Rel.bias values of both parameters are close to zero showing a

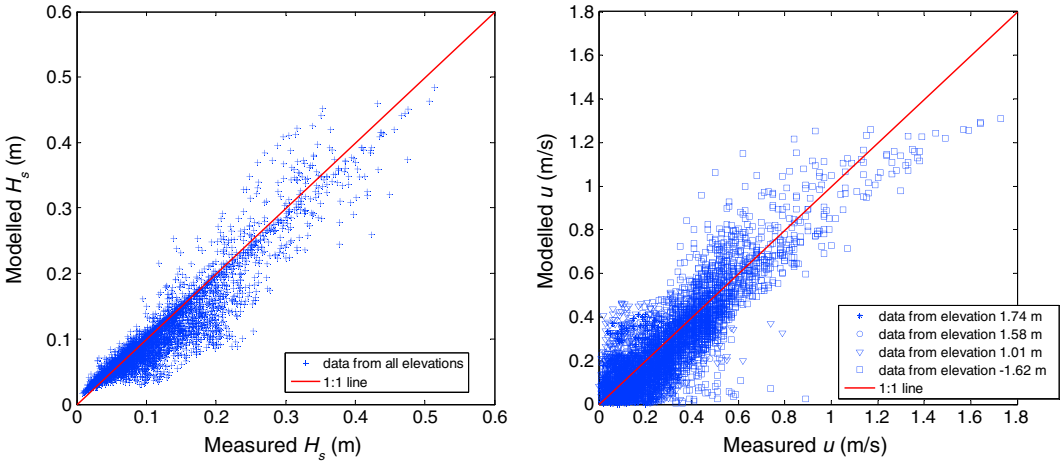


**Figure 3.** Hydrodynamic model performance in reproducing (left) $H_s$ and (right) $u$ against field measurements.

good model performance. It is noticed that the tidal current model underestimates the high current velocities at the most seaward measurement position (at −1.62 m NAP). However, this is not a problem for the present study as it has no effect on the BSS quantification on the upper tidal flat, where colonization might occur. This underestimation may be caused by the fact that the applied method does not count for the effect of horizontal shear, which transfers momentum from high-velocity zone (channels) to low-velocity zone (tidal flats). This effect is expected to be most apparent during spring tide when the tidal current velocity in the nearby channel is highest as shown in Figure 3. Since the other three monitoring profiles are not far from profile 25 (approximately 200 m to 1400 m; see Figure 2), it is assumed that the same hydrodynamic model and boundary conditions on profile 25 can also be applied on other profiles.

### 2.3.3. BSS Quantification

The validated hydrodynamic model was used to provide BSS data every half hour on the monitored four tidal flat profiles. This BSS assessment interval is chosen because the wave conditions provided by the wave pole in the estuary are measured every half hour. The magnitude of BSS induced by current is [*Roberts et al*., 2000]

$$\tau_{\text{cur}} = \rho f_c u_c^2 \tag{11}$$

where $\rho$ is water density, $f_c = g/C^2$, and $C$ is a Chézy coefficient determined as

$$C = 18\log_{10}(12h(x)/k_s) \tag{12}$$

$k_s$ is the Nikuradse roughness length $2.5 \times d_{50}$. The magnitude of wave induced BSS is [*Soulsby*, 1997]

$$\tau_{\text{wave}} = 0.5\rho f_w {u_{\text{wave}}}^2 \tag{13}$$

where $u_{\text{wave}}$ is the root-mean-square value of the maximum orbital motion near the bottom, which is outputted by the Simulating Waves Nearshore (SWAN) model. $f_w$ is a friction factor estimated as

$$f_w = 1.39\left(\frac{\xi}{k_s/30}\right)^{-0.52} \tag{14}$$

in which $\xi$ is particle excursion amplitude close to the bed, which was also a part of SWAN output. The mean BSS during a wave cycle under combined waves and currents is calculated as [*Soulsby*, 1997]

$$\tau_m = \tau_{\text{cur}}\left[1 + 1.2\left(\frac{\tau_{\text{wave}}}{\tau_{\text{cur}} + \tau_{\text{wave}}}\right)^{3.2}\right] \tag{15}$$

The maximum BSS during a wave cycle is calculated as [*Soulsby*, 1997]

$$\tau_{\text{max}} = \left[(\tau_m + \tau_{\text{wave}}|\cos\theta|)^2 + (\tau_{\text{wave}}|\sin\theta|)^2\right]^{0.5} \tag{16}$$

As $\tau_{\text{max}}$ is a measure of the peak hydrodynamic forcing, it is selected to be the representative BSS in the WoO1&WoO2 model, which directly influences seedlings survival prediction. To avoid the potential errors

related to very shallow water, $\tau_{max}$ is quantified only when the water depth is larger than 0.1 m. $\tau_{max}$ is assumed to be zero when the water depth is shallower than 0.1 m.

### 2.4. Calibration of WoO Models and Model Selection

In order to evaluate which WoO model is better supported by the observations, we first calibrated both models and then assess their performance by Akaike information criterion (AIC). The WoO1 model has only one calibration parameter, $t_{WoO1}$, while the WoO1&WoO2 model has three calibration parameters, $t_{WoO1}$, $t_{WoO2}$, and $k$. The calibration is done by tuning the parameters to minimize the total prediction errors of vegetation establishment pattern. Both observations and modeling outputs are expressed as 1/0 distributions. The errors are measured by residual sum of squares (RSS):

$$\mathrm{RSS} = \sum_{i=1}^{n} \left(\Psi^{i}_{\mathrm{model}} - \Psi^{i}_{\mathrm{obs}}\right)^2 \tag{17}$$

where $n$ is the number of segments in the potential pioneer zone on the four tidal flat transects in Figure 2. The three parameters in the WoO1&WoO2 model were tuned independently. $t_{WoO1}$ and $t_{WoO2}$ were varied at a half-day step, which resembles the semidiurnal tidal cycles.

It is noted that the two different vegetation establishment models have different degrees of complexity with the WoO1&WoO2 model being more complex than the other one. AIC accounts for both the model performance and model complexity represented by the number of calibration parameters [*Johnson and Omland*, 2004]. Greater model complexity is penalized to ensure a fair comparison between competing models. AIC quantification is carried out as

$$\mathrm{AIC} = n \ln(\mathrm{RSS}/n) + 2p \tag{18}$$

where $p$ is the number of calibration parameters representing the model complexity. A lower AIC score indicates a batter overall model performances. Based on the AIC scores, the probability that one model is the best model among the candidate models can be assessed by Akaike weights ($W_i$) [*Johnson and Omland*, 2004]:

$$W_i = \frac{\exp(-0.5 \times (\mathrm{AIC}_i - \mathrm{AIC}_{\mathrm{min}}))}{\sum_{j}^{R} \exp\left(-0.5 \times \left(\mathrm{AIC}_j - \mathrm{AIC}_{\mathrm{min}}\right)\right)} \tag{19}$$

where $R$ is the number of models, i.e., 2; $\mathrm{AIC}_{\mathrm{min}}$ is the minimum AIC score among a set models.

Like any statistical analysis, AIC assessment requires independent observations to avoid inflating statistical significance. However, observations of tidal flat segments are likely to be correlated with their neighboring segments resulting in spatial autocorrelation [*Fortin and Dale*, 2005]. In order to correct for the autocorrelation and obtain independent data sets, we subsampled the original vegetation establishment data set at an interval. This interval was determined as the minimum distance between two uncorrelated segments. The degree of correlation between two segments is measured using Moran's I [*Fortin and Dale*, 2005], which is a function of the distance ($d$) between the two segments. Moran's I ($I$) was calculated based on the minimum $k_e$ of each segment as it directly relates to the WoO occurrence:

$$I(d) = \frac{\frac{1}{W}\sum_{h=1}^{n}\sum_{i=1}^{n} w_{hi}\left(k_{e\_h} - \overline{k_e}\right)\left(k_{e\_i} - \overline{k_e}\right)}{\frac{1}{n}\sum_{i=1}^{n}\left(k_{e\_i} - \overline{k_e}\right)^2} \quad h \neq i \tag{20}$$

$k_{e\_h}$ and $k_{e\_i}$ are the minimum $k_e$ from segment $h$ and $I$; $\overline{k_e}$ is the spatial mean of the $k_e$ of all segments; $w_{hi}$ is a matrix of weighted values; and $w_{hi} = 1$, when $k_{e\_h}$ and $k_{e\_i}$ are from segments of a given distance ($d$). $w_{hi} = 0$ for all other cases. $W$ is the sum of the $w_{hi}$. When the $d \geq 5$ m, $I(d)$ drops below value $1/e$. It suggests that two segments are uncorrelated, if they are at least 5 m apart. Such distance is then defined as the interval to subsample the original data set for independent data. The overall AIC scores were determined by averaging the subsampled data sets.

### 2.5. Quantification of BSS and WoO on Schematized Profiles

In order to explore the influence of tidal flat bathymetry on vegetation establishment, we quantified WoO occurrence on schematized tidal flat profiles. A set of schematized profiles with varying slopes and contrasting

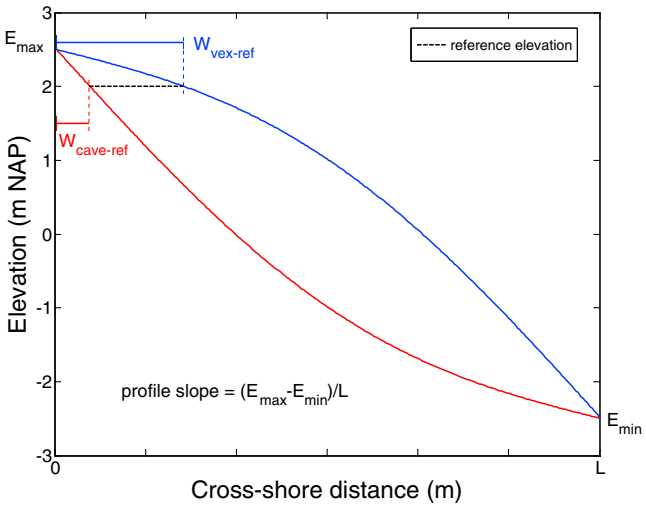


**Figure 4.** Schematized concave and convex tidal flat profiles. The demonstrated two profiles have the same slope as $(E_{max} - E_{min})/L$, where $E_{max}$ = 2.5 m NAP and $E_{min}$ = −2.5 m NAP, respectively, i.e., the elevation of the upper and lower ends of the tidal flats. A reference elevation is set to be 2 m NAP as an example; $W_{cave\text{-}ref}$ and $W_{vex\text{-}ref}$ are the reference salt marsh width for concave and convex profiles based on the reference elevation.

shapes was built. For each slope, a convex profile and a concave profile were tested to resemble tide- and wave-dominated tidal flats [*Friedrichs*, 2011]. These profiles were first descripted by a cosine function with amplitude being $A$ (m):

$$f(x) = A\cos\left(\frac{x}{L}\pi\right) \quad -\frac{L}{2} \le x \le \frac{L}{2} \qquad (21)$$

where $L$ is the width of the tidal flat profile. For convex profiles, $A = 1$. For concave profiles, $A = -1$. Second, the profiles were rotated around the origin to ensure that the upper and lower ends of the tidal flat profiles were $E_{max}$ and $E_{min}$ (Figure 4). In Figure 4, $E_{max}$ and $E_{min}$ are 2.5 m and −2.5 m, respectively. Then, profile slope is $(E_{max} - E_{min})/L$. By varying $L$ from 300 m to 1000 m, different profile slopes (1/60–1/200) can be achieved. In total, 16 tidal flat profiles with eight different slopes and two different profile shapes (convex or concave) were built.

The vegetation colonization pattern on these profiles was investigated using both the calibrated WoO1 and WoO1&WoO2 to further demonstrate the effect of including the WoO2. For both models, the lowest elevation for plant establishment (LE) and associated salt marsh width were quantified. LE is determined as the lowest elevation that has WoO events. Accordingly, salt marsh width is defined as the horizontal distance from profile upper ends till LE. In the WoO1&WoO2 model, time series of water level and wave conditions were provided by the data obtained at the study site to enable BSS quantification on these schematized profiles. When considering hydrodynamic forcing in WoO2, LE can vary with different profile morphology due to the different forcing environment and salt marsh width will vary accordingly. Assuming LE is constant on different profiles, salt marsh width is still different on these profiles because of the difference in profile configurations (Figure 4). In order to separate the variations in salt marsh width induced by the different forcing condition from those induced by different profile geometry, we defined a reference salt marsh width for each profile based on a single reference elevation (Figure 4). The difference between the reference salt marsh width and the salt marsh width derived from WoO1&WoO2 model is then the salt marsh width variation due to different forcing conditions. For concave profiles, the reference salt marsh width is $W_{cave\text{-}ref}$, whereas for convex profile, the reference salt marsh width is $W_{vex\text{-}ref}$. As the WoO1 model only considers the water level fluctuations, the LE on different profiles is expected to be constant regardless of the profile bathymetry. Therefore, the LE from the calibrated WoO1 model is selected to be the reference elevation (e.g., 2 m NAP in Figure 4).

## 3. Results

### 3.1. Vegetation Cover Monitoring

Semicontinuous vegetation cover monitoring using sequential aerial images shows that a sudden gain in vegetation area only occurred on profile 50 and profile 70 during the period 2004–2007 (Figures 5a and 5b). Using a Google Earth image further narrowed down the sudden vegetation recruitment in the period from 2004 to 2005. By tracing the leading salt marsh edge over time, information of salt marsh area dynamics on the four profiles can be obtained (Figures 5b–5f). On profiles 20 and 25, the leading salt marsh edge was moving shoreward with the retreating cliffs over the whole monitoring period. On profiles 50 and 70, the leading salt marsh edge also moved shoreward from 2001 to 2004 (Figures 5e and 5f). In 2004, however, there was seaward propagation of leading salt marsh edges due to sudden gains in

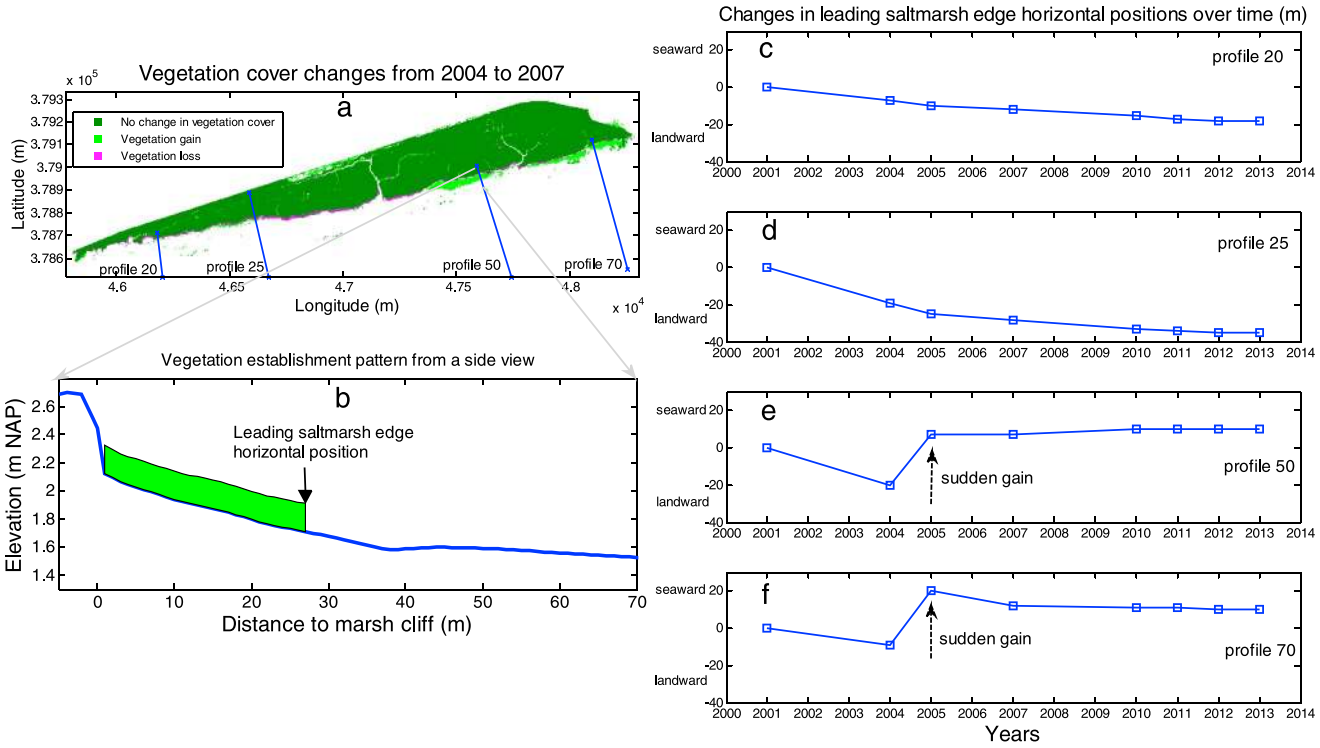


**Figure 5.** Vegetation cover changes monitoring. (a) Vegetation cover change from 2004 to 2007. (b) Side view of the vegetation area gain on profile 50. The solid black arrow indicates the leading salt marsh edge position in 2007, which was on the salt marsh cliff in 2004. (c–f) The changes in leading salt marsh edge horizontal positions on four profiles relative to the position in 2001.

vegetation areas, which was picked up by the observation in 2005. Afterward, the leading salt marsh edge on those two profiles became relatively stable. At the study site, the observed shoreward salt marsh edge migration may be trigged by storms, channel migration, and dredging activities [*Van der Wal et al.*, 2008]. The observed shoreward salt marsh edge migration is investigated in details by the two WoO models.

### 3.2. Time Series of BSS

In order to understand the relation between hydrodynamic disturbance and vegetation establishment pattern, BSS time series of each segment on the four monitoring profiles were quantified during the growing season (Figure 6). The fluctuations in the $\tau_{max}$ are induced by the covarying wave and tidal current conditions. Periods with zero BSS in the time series are due to shallow water inundation (water depth $< 0.1$ m) during neap tide. For the demonstrated elevation (1.85 m NAP), there are multiple long inundation-free periods ($t_{WoO1} = 2.5$ days) in both growing seasons of 2004 and 2012. Subsequent to these periods, $k_e$ can be derived to represent the BSS time series in a WoO2 and compared with a calibrated $k$ ($5.9 \times 10^{-4}$ Pa/h), which represents seedling BSS tolerance. The three parameters $t_{WoO1}$, $t_{WoO2}$, and $k$ were determined by calibration, which is described in the following section. In 2004, $k_e$ varies from $5.0 \times 10^{-4}$ Pa/h to $4.7 \times 10^{-3}$ Pa/h. It is noted that $k_e$ is lower than the calibrated $k$ in the WoO2 period around 1 June 2004 (indicated in green in Figure 6). In 2012, however, all three $k_e$ in WoO2 exceed the calibrated $k$ value. The difference in the BSS time series (represented by $k_e$) in these two years will lead to different vegetation establishment outcome at this elevation, which is further elaborated in the following section.

### 3.3. WoO Models Calibration and Evaluation

The two vegetation establishment models were calibrated against the monitored vegetation cover dynamics from two contrasting years: 2004 and 2012 (Figure 7). Observation from 2004 was selected for model calibration as the colonization occurred in this year. In this year, the elevation of profiles 20 and 25 was too low to have potential pioneer zone (above 1.7 m NAP). However, there were potential pioneer zones on profiles 50 and 70. They were colonized from the salt marsh cliff till 27 m and 21 m seaward,

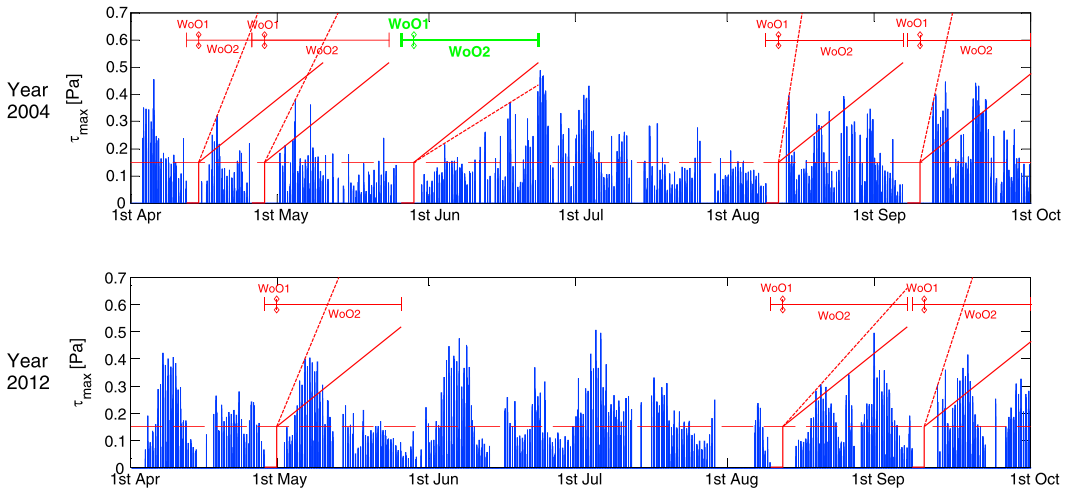


**Figure 6.** Example of $\tau_{max}$ time series (blue bars) in the growing season (1 April to 1 October) of year 2004 and 2012 from elevation 1.85 m NAP on profile 50. $\tau_{max}$ is the maximum wave-current BSS in a wave period. "WoO1" indicates an inundation-free period $t_{WoO1} = 2.5$ days ($\tau_{max} = 0$), and "WoO2" indicates a period with $t_{WoO2} = 25.5$ days. The red solid line is the calibrated $\tau_{veg}$ function with $k = 5.9 \times 10^{-4}$ Pa/h. These three parameters $t_{WoO1}$, $t_{WoO2}$, and $k$ were determined by model calibration in section 3.3. The thick red dashed line indicates $k_e$ derived from $\tau_{max}$ time series. Only during a period around 1 June 2004, $k_e < k$, i.e., $\tau_{max}$ stays lower than $\tau_{veg}$ during the whole WoO2. Thus, this period (WoO1 and WoO2) may lead to salt marsh recruitment, which is indicated in green. In other periods of both years when $k_e > k$, seedlings may not surpass the WoO2 with high disturbance magnitude. These periods are then indicated in red. The horizontal dashed line indicates $\tau_{sed}$. $\tau_{max}$ is only quantified when water depth is higher than 0.1 m to avoid unrealistic BSS predictions associated with very shallow water. When the water depth is shallower than 0.1 m, BSS is assumed to be zero. For some cases, BSS is zero, but tidal inundation (<0.1 m) is still present, which prevents WoO1 occurrence (e.g., the period around 1 August 2012).

respectively. Data from 2012 were selected to be the other part of data set for the model calibration. This year is selected because new potential pioneer zones emerged in front of salt marsh cliffs or previously colonized areas on all profiles, but they stayed bare despite of the suitable elevation, which is contrasting to the vegetation colonization in 2004. The vegetation cover dynamics in other years are not included in the model calibration because of the limited changes in salt marsh area (Figure 5) or the lack of profile bathymetry data in those years.

The predictions of the WoO1 model and WoO1&WoO2 model were evaluated based on the overall vegetation cover dynamics in 2004 and 2012 (Figure 7). If $t_{WoO1}$ is set to be 5 days, the WoO1 model can predict the observed establishment in 2004 reasonably well ("pre-5 days" in Figure 7, middle row). However, this setting leads to large overestimations of plant establishment in 2012 (pre-5 days in Figure 7, bottom row). If $t_{WoO1}$ is set to be 6 days, the WoO1 model has the best fit of the overall observations ("pre-6 days" in Figure 7). In general, pre-6 days underestimates the plant establishment areas in 2004 and overestimates the areas in 2012. Because $t_{WoO1}$ is increased by 1 day from pre-5 days to pre-6 days, the predicted colonization areas were reduced. Pre-best is the prediction from the best fitted WoO1&WoO2 model (Figure 7). It can capture the establishment events in 2004 reasonably well despite an overestimation on the profile 70. In addition, it also predicts the absence of plants establishment at the potential pioneer zone on all the four profiles in 2012, which is in a good agreement with the observations. Moreover, there was no establishment in both years on profiles 20 and 25. This can be explained by the WoO1&WoO2 model as follows: in 2004, when the external condition was favorable for establishment, the elevation on those two profiles was too low to facilitate establishments, and in 2012, however, when the profiles had reached adequate elevation, the external conditions became unfavorable.

Based on the vegetation cover changes in 2004 and 2012 on the four profiles, model selection procedure using AIC indicates that the WoO1&WoO2 model is better supported compared to the WoO1 model (Table 1). The total number of observation points ($n$) is 193, i.e., number of segments in the potential pioneer zone in those two years. Pre-best derived from the best fitted WoO1&WoO2 model results in minimum errors (RSS = 19) among the three predictions. After penalizing for the greater model complexity, the best fitted WoO1&WoO2 model still has the lowest AIC score and its Akaike weight is as high as 1,

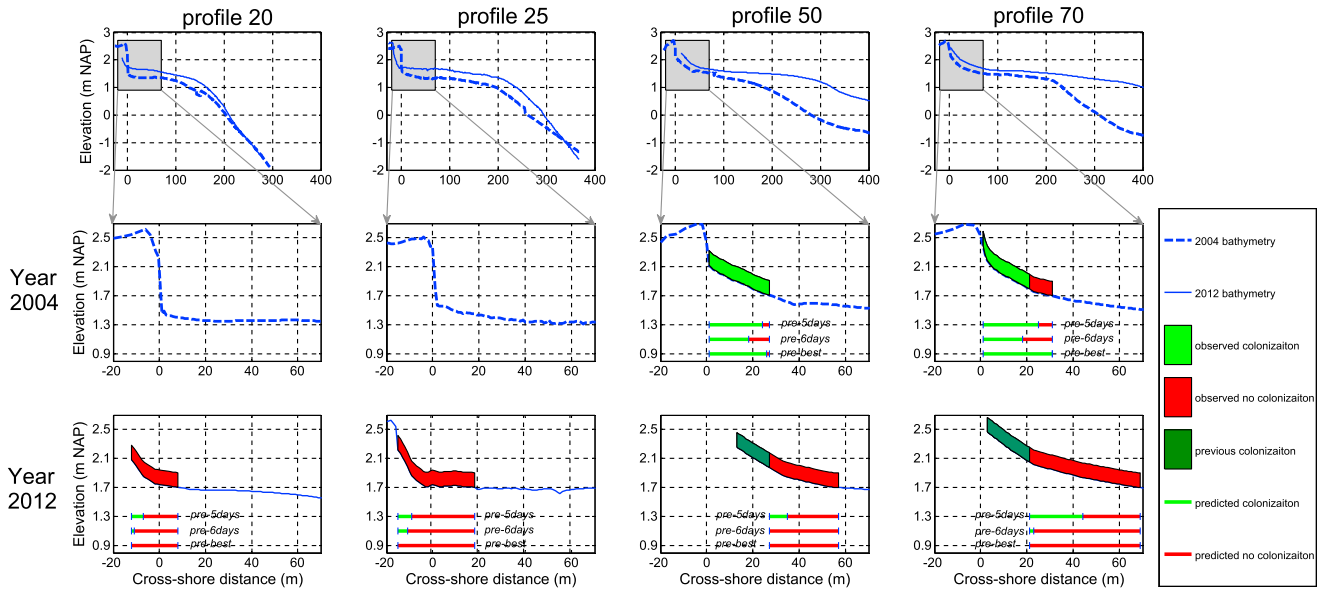


**Figure 7.** Observations and predictions on vegetation establishment pattern on the four monitored tidal flat profiles in 2004 and 2012. (top row) Bathymetry of the four profiles. The shaded areas in these panels are enlarged in Figure 7 (middle and bottom rows). The vegetation cover monitoring and predictions are also shown for (middle row) 2004 and (bottom row) 2012. For all the profiles, 1.7 m NAP is the suggested threshold elevation suggested by *Wang and Temmerman* [2013], above which the shift from a bare state to vegetated state is likely to occur. The areas above this threshold till marsh cliffs are regarded as potential pioneer zones. Vegetation establishment observations and predictions were confined in these areas. Three predictions are included: pre-5 days is the prediction of the WoO1 model with $t_{WoO1} = 5$ days; pre-6 days is the prediction of the WoO1 model with $t_{WoO1} = 6$ days; and pre-best is the best fit results based on WoO1&WoO2 model. Details of the parameter settings and model evaluation are shown in Table 1. Colonization from previous period (in 2004) is not included in the vegetation establishment modeling in 2012.

indicating that this model is unambiguously supported by the data despite its higher degree of model complexity. It is noted that the total length of a $t_{WoO1}$ and $t_{WoO2}$ is 28 days, which is the duration of two spring-neap tidal cycles.

### 3.4. Sensitivity Analysis of *k*

The parameter *k* is the increase rate of $\tau_{veg}$ for salt marsh plants (i.e., the resistance against BSS disturbance), which has not yet been reported in the literature due to the still recent discovery of the WoO concept. Considering the uncertainty of *k*, a sensitivity analysis was carried out to test if the WoO1&WoO2 model prediction varies greatly with different *k*. The sensitivity analysis is done by quantifying the ratio of the predicted colonization area over the potential pioneer zone area using the WoO1&WoO2 model (Figure 8). The ratio can be visualized as the ratio of a horizontal green bar length of pre-best in Figure 7 over the whole bar length. The increase of *k* means that vegetation can increase $\tau_{veg}$ faster and the ratio of colonization area increases accordingly.

The sensitivity analysis shows that the overall model prediction (four profiles in two years) does not vary significantly if *k* deviates approximately 15% from the best fitted value ($4.9 \times 10^{-4}$ Pa/h to $6.9 \times 10^{-4}$ Pa/h) and that the prediction is generally in agreement with the observations (Figures 7 and 8). In 2004, there was no potential pioneer zone on profiles 20 and 25. Those two profiles in 2004 are then excluded in the sensitive analysis. On profiles 50 and 70 in 2004, it is predicted that a large portion of the potential pioneer

**Table 1.** Parameter Settings in Vegetation Establishment Predictions and Akaike Information Criterion (AIC) Analysis Based on the Overall Vegetation Cover Change Data From 2004 and 2012 on Four Monitoring Profiles

| Prediction | Model | Number of Parameters | WoO1 Duration (days) | WoO2 Duration (days) | *k* (Pa/h) | RSS/*n* | AIC | Akaike Weight |
|---|---|---|---|---|---|---|---|---|
| Pre-5 days | Only WoO1 | 1 | 5 | - | - | 56/193 | −44.42 | 0 |
| Pre-6 days | Only WoO1 (best fit) | 1 | 6 | - | - | 30/193 | −68.14 | 0 |
| Pre-best | WoO1&WoO2 (best fit) | 3 | 2.5 | 25.5 | $5.9 \times 10^{-4}$ | 19/193 | −81.50 | 1.00 |

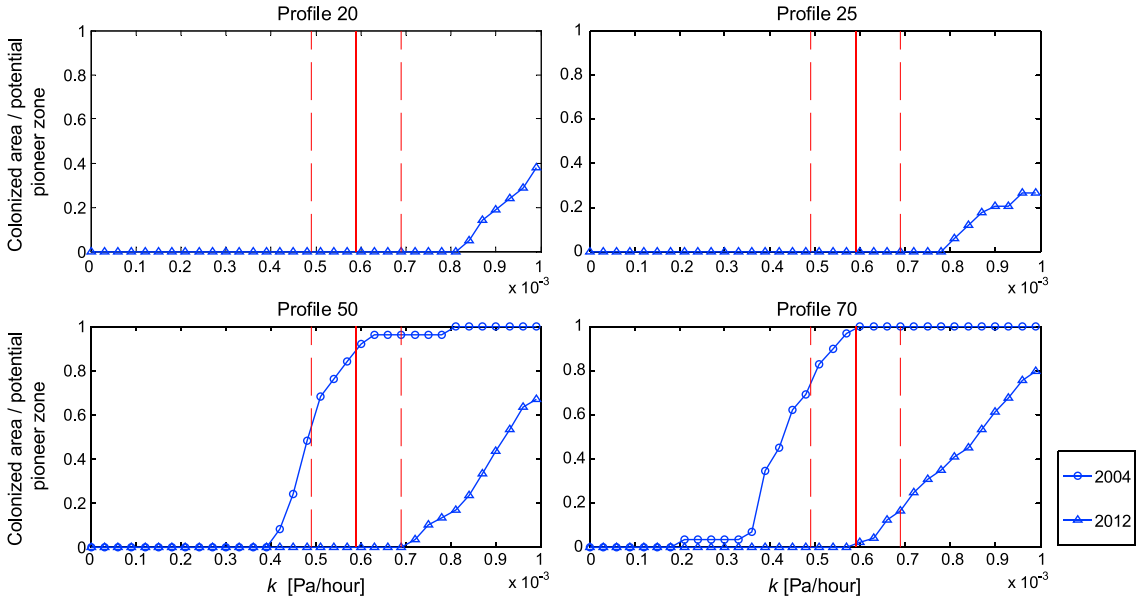


**Figure 8.** Ratio between vegetation-colonized area over the potential pioneer zone with varying $k$, obtained by the WoO1&WoO2 model. The ratio can be visualized as the ratio of a horizontal green bar length of pre-best in Figure 7 over the whole bar length. The best fitted $k$ value is $5.9 \times 10^{-4}$ Pa/h, which is indicated as the red solid line. The two red dashed lines indicate $k = 4.9 \times 10^{-4}$ Pa/h and $k = 6.9 \times 10^{-4}$ Pa/h, which is about 15% lower and higher than the best fitted $k$, respectively. There was no potential pioneer zone on profiles 20 and 25 in 2004, which is excluded in the sensitive analysis.

zone was colonized as long as $k$ is in the range of $4.9 \times 10^{-4}$ Pa/h to $6.9 \times 10^{-4}$ Pa/h, which generally agrees with the observations (Figure 8). In 2012, within the same range of $k$, it is predicted that there is no colonization on all profiles except profile 70, which is also similar with the observations.

### 3.5. BSS Distribution and Vegetation Establishment Pattern on Schematized Profiles

Based on the simple 1-D hydrodynamic model, we show that the distribution of $\tau_{wave}$ on different profiles is affected by their bathymetry, whereas the distribution of $\tau_{cur}$ is not influenced by profile bathymetry but only determined by the elevation (Figure 9a). The $\tau_{cur}$ decreases linearly with the increasing elevation and results in similar magnitude of BSS on both profiles. However, $\tau_{wave}$ on a gentle convex profile is lower than that on a steep concave profile, even with the same incident wave conditions. The difference is greater in the potential pioneer zone (i.e., zone where elevation $>$ 1.7 m NAP), which may lead to different seedling establishment patterns. The peak of $\tau_{wave}$ is where the waves are breaking. From seaward boundary to the wave breaking point, $\tau_{wave}$ becomes stronger with the increasing elevation (decreasing water depth) and the difference of $\tau_{wave}$ on two profiles also becomes more apparent. The location and the magnitude of the $\tau_{wave}$ peak are related to wave propagation processes on the tidal flat foreshore [*Green and Coco*, 2014].

The difference in $\tau_{wave}$ distribution leads to different $\tau_{max}$ in the potential pioneer zone (i.e., zone where elevation $>$ 1.7 m NAP) on the schematized profiles (Figures 9a and 9b). In such area, $\tau_{wave}$ on gentle convex profiles is generally lower than that on steep concave profiles. The $\tau_{max}$ on the gentlest convex profile and that on steepest concave profile become the two extremes with the lowest and highest forcing. The different magnitude of $\tau_{max}$ in the potential pioneer zones can influence the predicted vegetation establishment patterns in the WoO1&WoO2 model.

The lowest elevation for plants establishment (LE) was predicted to be 1.90 m NAP on all the profiles by the best fitted WoO1 model (Figure 10a). However, the WoO1&WoO2 model predicts that LE varies with profile slope and shape (Figure 10a). LE becomes lower as the profile slope becomes gentler. For concave and convex profiles, the LE is reduced by 0.32 m and 0.14 m, respectively, when the profile slope drops from 1/60 to 1/200. Furthermore, with the same profile slope, a convex profile has lower LE than the corresponding concave profile. The difference in LE becomes smaller as the profiles become gentler. Overall, the LE is lower on the profiles with lower $\tau_{max}$ (Figures 9 and 10b).

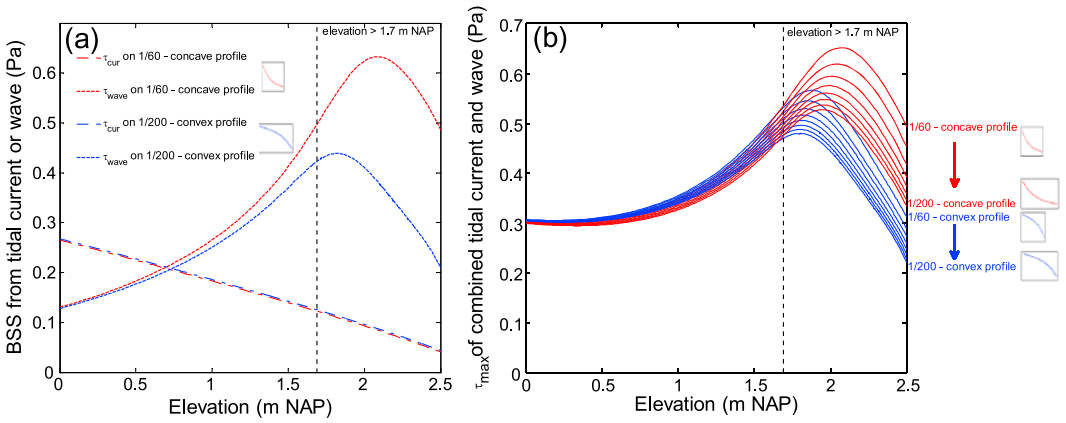


**Figure 9.** Example of BSS distribution over elevation on schematized tidal flat profiles. (a) Distributions of $\tau_{cur}$ and $\tau_{wave}$ on two contrasting tidal flat profiles: steepest concave profile (slope = 1/60) and gentlest convex profile (slope = 1/200). (b) Distribution of $\tau_{max}$ on all the schematized profiles with varying slope (1/60, 1/80, 1/100, 1/120, 1/140, 1/160, 1/180, and 1/200) and contrasting shapes. The BSS on convex profiles is indicated by blue lines, whereas the BSS on concave profiles is indicated by red lines. The potential pioneer zones (elevation > 1.7 m NAP) are indicated by the dotted line. The insert figures indicate the schematized profiles. The BSS was obtained when tidal level = 2.78 m NAP, $H_s$ = 0.53 m, and $T_p$ = 2.8 s.

Corresponding to the LE variations, the salt marsh width differs on the schematized profiles (Figure 10b). In order to examine the salt marsh width variation induced by LE variations (forcing conditions), the derived salt marsh width from WoO1& WoO2 modeling is compared to the reference pioneer zone widths ($W_{cave\text{-}ref}$ or $W_{vex\text{-}ref}$) based on a reference elevation at 1.9 m NAP. The reference elevation is derived from the best fitted WoO1 model. It is noted that both derived salt marsh width and reference pioneer zone widths increase with the decreasing profile slope. The increase of the reference pioneer zone widths is due to the profile difference itself, which is also inherent in the increase of the derived salt marsh width (Figure 10b). However, the difference between the derived salt marsh width and the reference pioneer zone widths is due to the different forcing environments provided by different tidal profiles, which is related to LE. As the profile slope decreases, LE becomes lower and the difference between the predicted salt marsh width and reference salt marsh width becomes larger. Such difference is larger on the convex profiles than that on

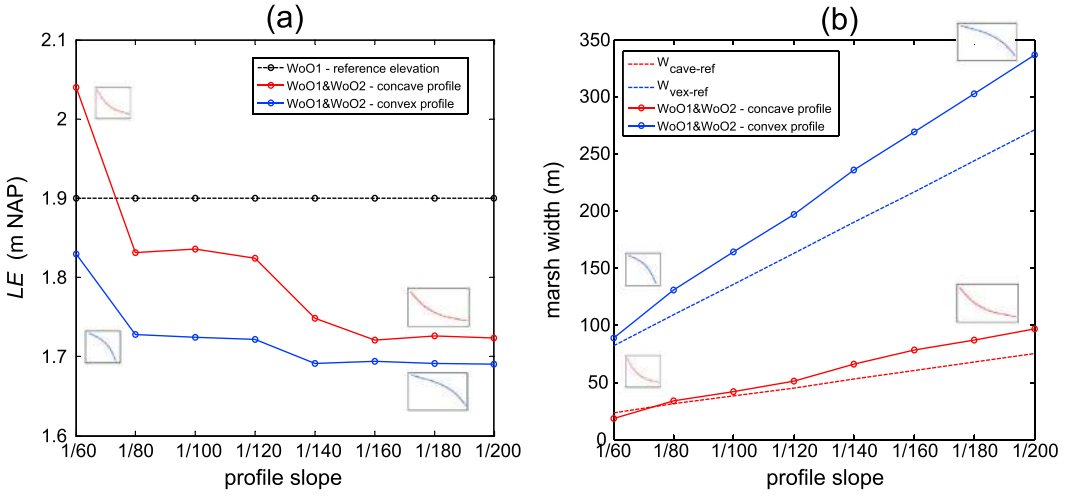


**Figure 10.** The variation of (a) lowest elevation for salt marsh establishment (LE) and (b) salt marsh width with schematized profile slope and shape. The solid blue and red lines are LE and salt marsh width results on different profiles using WoO1&WoO2 model. $W_{cave\text{-}ref}$ and $W_{vex\text{-}ref}$ are reference pioneer zone width of concave and convex profiles using a constant LE equals to 1.9 m NAP as suggested by the WoO1 model. The insert figures indicate the schematized profile bathymetry.

the concave profiles. This is because the upper part of the convex profile is very flat (small local slope) and a small variation in elevation may lead to large variation in horizontal distance. Distinctively, salt marsh width on the convex profile with the minimum slope is 337 m, which exceeds the corresponding $W_{vex\text{-}ref}$ by 66 m, i.e., an extra gain in the salt marsh pioneer zone as large as 24% of the $W_{vex\text{-}ref}$.

## 4. Discussion

Monitoring vegetation cover over time shows that vegetation colonization at the study site is episodic rather than gradual, as have been reported in previous studies [*Wang and Temmerman*, 2013; *Balke et al*., 2014]. This episodic expansion highlights the need of pinpointing the key mechanism that enable or inhibit vegetation survival and establishment. The windows of opportunity (WoO) concept provides a framework to understand the occurrence and absence of such colonization events with the external forcing [*Balke et al*., 2014]. Within this study, we show (i) that this WoO concept can be improved by incorporating more than one process-based WoO and (ii) how the derived establishment model can be used to mechanistically explain the relation between salt marsh establishment extent and tidal flat bathymetry.

### 4.1. The Importance of Hydrodynamic Forcing on Salt Marsh Establishment

To illustrate the principle of the WoO concept among various ecosystems, *Balke et al*. [2014] focused only on the disturbance frequency (i.e., inundation period). For simplicity sake and as a first step, they ignored the influence of the inherent disturbance magnitude (e.g., hydrodynamic forcing). Our study revealed that including additional disturbance magnitude leads to understand the causes of spatial and temporal variability in colonization events (Figures 5 and 7). The model incorporates both disturbance frequency and disturbance magnitude in two consecutive WoOs and explained the vegetation recruitment significantly better. This suggests that seedlings not only need to time their initial establishment, set by Wo1, but also need to "outgrow" the hydrodynamic disturbance, set by WoO2, in order to become successfully established. This finding highlights the regulation effect of hydrodynamics on the seedling survivals, which is in line with the previous field and laboratory studies [*Bouma et al*., 2009; *Schwarz et al*., 2011; *Balke et al*., 2011]. Tidal flat morphodynamic models have shown that the biogeomorphic feedbacks between morphological development and vegetation dynamics are important for the long-term tidal ecosystem evolution [*Fagherazzi et al*., 2012; *Mariotti and Fagherazzi*, 2010; *Temmerman et al*., 2007; *van de Koppel et al*., 2005]. The sediment transport process in these studies is often treated in detail by morphodynamic models (e.g., Delft3D in *Temmerman et al*. [2007]), but the processes related to vegetation establishment and loss are generally described in an aggregated way. Our salt marsh establishment model, however, explicitly considers the mechanisms that enable and disable salt marsh establishment. This will help in understanding the consequences of biogeomorphic feedbacks and predicting long-term trajectory in tidal flat morphodynamic models.

It is noted that the proposed WoO1&WoO2 model only accounts for the timing and the magnitude of the BSS disturbance (as shown in Figure 1), whereas the duration when the BSS around seedlings is above $\tau_{sed}$ is not considered. This duration is relevant for seedling establishment process, as it determines how much sediment can be eroded or suspended from the bed. If the duration is long enough, the sediment around seedling root can be removed completely, which leads to seedling dislodgement. However, for simplicity sake, the present model ignored the effect of the duration with high BSS ($> \tau_{sed}$) as a first step to explore the importance of hydrodynamic forcing in salt marsh recruitment modeling.

### 4.2. Potential Consequences of Tidal Flat Bathymetry for Salt Marsh Management and Restoration

The WoO1&WoO2 model predicts that salt marsh establishment elevation (LE) varies with the profile morphology, whereas the WoO1 model and the empirical description in *Wang and Temmerman* [2013] predict that salt marsh establishment elevation is constant on different profiles as long as the tide fluctuation is the same. It is shown that tidal flat morphology determines the LE for vegetation establishment by affecting hydrodynamic forcing and thereby affects the overall salt marsh extent (Figures 9 and 10). Specifically, the difference in attenuating wave forcing on different tidal flat morphologies will lead to different vegetation establishment patterns. These insights give handles to develop effective conservation and restoration practices for salt marsh ecosystems.

Salt marsh restoration and conservation projects normally aim for creating or preserving salt marsh zone with a sufficient width over a range of elevations to optimize the associated ecosystem services, e.g., habitat provision and wave attenuation [*Barbier et al*., 2008; *Borsje et al*., 2011; *Hu et al*., 2014]. The vegetation establishment modeling on schematized profiles provides three valuable general applicable rules for restoration projects. First, it is apparent that convex and gentler profiles are more favorable in hosting large areas of salt marsh compared to concave and steeper profiles (Figure 10b). Hence, when selecting potential salt marsh restoration sites, not only the elevation zone in an intertidal frame but also tidal flat morphology and associated wave attenuation should be considered, which is also noted in *Winterwerp et al*. [2013] and *Anthony and Gratiot* [2012] for mangrove establishment. Second, wave forcing is more efficiently dissipated on convex (tide-dominated) profiles than concave (wave-dominated) profiles because the higher foreshore elevation leads to higher dissipation and longer distance from wave breaking points toward the potential pioneer zone (Figure 9). This leads to lower elevation of the salt marsh edge and gain in salt marsh area (Figures 9 and 10). Therefore, it is beneficial to create more dissipative foreshores of suitable sites, for example, by disposing dredging materials [*Temmerman et al*., 2013]. At locations with benign hydrodynamic forcing, putting dredged sediment can further increase the sediment supply to promote salt marsh accretion and new salt marsh establishment [*Day et al*., 2007; *Temmerman et al*., 2013]. Third, dredging activities near tidal flats should be very cautious, as unexpected loss in potential salt marsh pioneer area may occur if the bathymetry is altered to be less efficient in dissipating wave energy. Hence, comprehensive assessment of the dredging and dumping activities near marshes is necessary.

### 4.3. Potential Consequences of Changing Boundary Conditions

The hydrodynamic forcing experienced within the pioneer zone is of course strongly influenced by the seaward boundary condition (incident wave height, current velocity, etc.). It would be interesting to explore how seedling establishment patterns adjust to long-term boundary condition variations, e.g., the long-term increase of storminess due to climate change [*Day et al*., 2008; *Donat et al*., 2011]. However, such long-term trend analyses may not provide input with a sufficient high temporal resolution (e.g., every 30 min) as needed for applying the WoO1&WoO2 model. Nevertheless, our results imply that there may be "snowball" effects in the relation between salt marsh establishment opportunity and hydrodynamic boundary variations [*Winterwerp et al*., 2013; *Anthony and Gratiot*, 2012]. For example, an increase in storminess due to climate change may directly lead to more hostile forcing environment for seedling survival [*Day et al*., 2008; *Donat et al*., 2011; *Balke et al*., 2013]. Additionally, increased wave forcing can lead to more concave tidal flats [*Friedrichs*, 2011]. Therefore, the hostile forcing environment is amplified by the fact that the profile is becoming less dissipative, making the switch back to a favorable condition for establishment even more difficult.

### 4.4. The Importance of Plant Growth and Environmental Characteristics for Establishment

In the WoO1&WoO2 model, we used a linear increase rate $k$ to describe how growing seedlings increase their tolerance to $\tau_{max}$, due to the seedling root growth [*Balke et al*., 2011; *Infantes et al*., 2011]. Similarly, such increase rate has been estimated for mangrove seedlings by *Balke et al*. [2011]. However, their estimation for mangrove seedlings ($3.3 \times 10^{-3}$ Pa/h) is much higher than the calibrated rate $k$ we obtained for salt marsh plants ($5.9 \times 10^{-4}$ Pa/h). This difference may be induced by the fact that mangroves are the tropical species with diapsores and therefore have an inherently much higher (root) growth rate than temperate salt marsh plants [*Saintilan et al*., 2014]. In reality, the actual occurring seedling root growth is also influenced by various abiotic factors such as temperature, salinity, and substrate substance [*Mudd et al*., 2009; *Kirwan and Guntenspergen*, 2012; *Booth and Loheide*, 2012]. Thus, $k$ may be a spatial-temporal variable depending on the above mentioned factors. Further field and laboratory studies are needed to provide better estimates of $k$ for various species and various growth conditions. Nevertheless, our sensitivity analysis suggests that the occurrence of vegetation establishment events is not significantly altered if abiotic factors vary within a reasonable range, indicating that the uncertainty in $k$ does not greatly affect model robustness in describing the observed vegetation establishment patterns.

In the current setting of the WoO1&WoO2 model, the duration of WoO1 may influence the seedlings tolerance and the duration of WoO2. As WoO1 is the period when seedlings experience no disturbance, it is expected that the longer the WoO1 is, the better seedlings can grow (with deeper roots). Correspondingly, the duration of WoO2, as the required low disturbance period, can be shorter to ensure

the successful establishment. However, in the present study, the duration of WoO1 and WoO2 is derived by model calibration. The actual influence of WoO1 duration on WoO2 and plant tolerance may be better assessed by further experiments.

### 4.5. Applying the WoO1&WoO2 Model

In the present study, the model is applied to a mesotidal to macrotidal tidal flat. For microtidal tidal flats and lakeside marshes, the proposed WoO1&WoO2 model is still applicable, where the BSS induced by wind waves can be more important compared to the tidal currents [e.g., *D'Alpaos et al*., 2013; *Green and Coco*, 2014]. To apply the WoO1&WoO2 model in other cases, accurate hydrodynamic modeling and in situ hydrodynamic boundary conditions are needed. In different environments, BSS quantification can be delivered by other (more complex) hydrodynamic models, but the core of the WoO recruitment concept remains the same. In this study, BSS quantification was ensured by the validated hydrodynamic model that accounts for the combined effect of current and waves (Figure 3). Hydrodynamic boundary conditions for modeling were provided by the long-term water level and wave measurements from the nearby stations. Such a method relies on archived data and empirical relations to derive the in situ hydrodynamic conditions of the past period. However, it cannot provide the hydrodynamic conditions, especially the more unpredictable wave conditions in the future, which are essential to BSS time series quantification.

A recent study has shown that the occurrence of BSS exceeding a given threshold in subtidal and intertidal areas can be modeled as a marked Poisson processes, in analogy with the occurrence of precipitation [*D'Alpaos et al*., 2013]. The interarrival times, intensities, and durations of these events are exponentially distributed. Therefore, based on the statistical characterization of the previous period, BSS time series can be generated via Monte Carlo realizations for WoO1&WoO2 model predictions of the future period. That is, the salt marsh establishment possibility can be predicted for the incoming period (e.g., 5–10 years) based on the existing BSS and tidal inundation data, which is valuable to the salt marsh conservation and restoration projects.

## 5. Conclusions

In this study, we revealed that including hydrodynamic forcing (as disturbance magnitude) in the WoO concept is important for understanding and predicting vegetation establishment process. The WoO1&WoO2 model, which considers both the disturbance frequency (WoO1) and the disturbance magnitude (WoO2), can explain the observed vegetation establishment patterns on a tidal flat. This model offers a tool to understand vegetation establishment mechanisms and can predict salt marsh restoration success under contrasting conditions. Applying this model on contrasting tidal flat profiles shows that salt marsh plant establishment patterns are influenced by the foreshore bathymetry and related wave force distribution. Gentle convex profiles are more effective in dissipating wave forcing than steep concave profiles, which leads to wider elevation range and larger area for seedling establishment. Therefore, salt marsh restoration and management projects should seek not only for suitable accommodating elevations but also favorable foreshore morphology to maximize the vegetation establishment opportunities. Thus, affecting the tidal flat morphology can open up windows of opportunity to restore and manage these valuable coastal ecosystems.

**Acknowledgments**
The data in this paper are available upon request from the author. This study has been supported by Technology Foundation STW with project 07324/ BEB. 7324. We thank Rijkswaterstaat (Jan van het Westende and Marco Schrijver) for providing current velocity data and aerial photos. We also thank Lennart van IJzerloo, Jeroen van Dalen, Jos van Soelen, and Annette Wielemaker for their help in field work and data processing.

## References

Allen, J. R. L. (1995), Salt-marsh growth and fluctuating sea level: Implications of a simulation model for Flandrian coastal stratigraphy and peat-based sea-level curves, *Sediment. Geol.*, *100*(1–4), 21–45, doi:10.1016/0037-0738(95)00101-8.

Anthony, E. J., and N. Gratiot (2012), Coastal engineering and large-scale mangrove destruction in Guyana, South America: Averting an environmental catastrophe in the making, *Ecol. Eng.*, *47*, 268–273, doi:10.1016/j.ecoleng.2012.07.005.

Balke, T., T. J. Bouma, E. M. Horstman, E. L. Webb, P. L. A. Erftemeijer, and P. M. J. Herman (2011), Windows of opportunity: Thresholds to mangrove seedling establishment on tidal flats, *Mar. Ecol. Prog. Ser.*, *440*, 1–9.

Balke, T., T. J. Bouma, P. M. J. Herman, E. M. Horstman, C. Sudtongkong, and E. L. Webb (2013), Cross-shore gradients of physical disturbance in mangroves: Implications for seedling establishment, *Biogeosciences*, *10*(8), 5411–5419, doi:10.5194/bg-10-5411-2013.

Balke, T., P. M. J. Herman, and T. J. Bouma (2014), Critical transitions in disturbance-driven ecosystems: Identifying windows of opportunity for recovery, *J. Ecol.*, *102*(3), 700–708, doi:10.1111/1365-2745.12241.

Barbier, E. B., et al. (2008), Coastal ecosystem-based management with nonlinear ecological functions and values, *Science*, *319*(5861), 321–323, doi:10.1126/science.1150349.

Bearman, J. A., C. T. Friedrichs, B. E. Jaffe, and A. C. Foxgrover (2010), Spatial trends in tidal flat shape and associated environmental parameters in South San Francisco Bay, *J. Coast. Res.*, *26*(2), 342–349.

Booij, N., R. C. Ris, and L. H. Holthuijsen (1999), A third-generation wave model for coastal regions: 1. Model description and validation, *J. Geophys. Res.*, *104*(C4), 7649–7666, doi:10.1029/98JC02622.
Booth, E. G., and S. P. Loheide (2012), Hydroecological model predictions indicate wetter and more diverse soil water regimes and vegetation types following floodplain restoration, *J. Geophys. Res.*, *117*, G02011, doi:10.1029/2011JG001831.
Borsje, B. W., B. K. van Wesenbeeck, F. Dekker, P. Paalvast, T. J. Bouma, M. M. van Katwijk, and M. B. de Vries (2011), How ecological engineering can serve in coastal protection, *Ecol. Eng.*, *37*(2), 113–122.
Bouma, T. J., M. Friedrichs, P. Klaassen, B. K. Van Wesenbeeck, F. G. Brun, S. Temmerman, M. M. Van Katwijk, G. Graf, and P. M. J. Herman (2009), Effects of shoot stiffness, shoot size and current velocity on scouring sediment from around seedlings and propagules, *Mar. Ecol. Prog. Ser.*, *388*, 293–297, doi:10.3354/meps08130.
Cahoon, D. R., P. F. Hensel, T. Spencer, D. J. Reed, K. L. McKee, and N. Saintilan (2006), Coastal wetland vulnerability to relative sea-level rise: Wetland elevation trends and process controls, in *Wetlands and Natural Resource Management*, pp. 271–292, Springer, New York.
Callaghan, D. P., T. J. Bouma, P. Klaassen, D. van der Wal, M. J. F. Stive, and P. M. J. Herman (2010), Hydrodynamic forcing on salt-marsh development: Distinguishing the relative importance of waves and tidal flows, *Estuarine Coastal Shelf Sci.*, *89*(1), 73–88.
Carniello, L., A. Defina, S. Fagherazzi, and L. D'Alpaos (2005), A combined wind wave-tidal model for the Venice lagoon, Italy, *J. Geophys. Res.*, *110*, F04007, doi:10.1029/2004JF000232.
Carniello, L., A. D'Alpaos, and A. Defina (2011), Modeling wind waves and tidal flows in shallow micro-tidal basins, *Estuarine Coastal Shelf Sci.*, *92*(2), 263–276, doi:10.1016/j.ecss.2011.01.001.
D'Alpaos, A., L. Carniello, and A. Rinaldo (2013), Statistical mechanics of wind wave-induced erosion in shallow tidal basins: Inferences from the Venice Lagoon, *Geophys. Res. Lett.*, *40*, 3402–3407, doi:10.1002/grl.50666.
Day, J. W., Jr., et al. (2007), Restoration of the Mississippi Delta: Lessons from Hurricanes Katrina and Rita, *Science*, *315*(5819), 1679–1684, doi:10.1126/science.1137030.
Day, J. W., R. R. Christian, D. M. Boesch, A. Yáñez-Arancibia, J. Morris, R. R. Twilley, L. Naylor, L. Schaffner, and C. Stevenson (2008), Consequences of climate change on the ecogeomorphology of coastal wetlands, *Estuaries Coasts*, *31*(3), 477–491, doi:10.1007/s12237-008-9047-6.
Donat, M. G., D. Renggli, S. Wild, L. V. Alexander, G. C. Leckebusch, and U. Ulbrich (2011), Reanalysis suggests long-term upward trends in European storminess since 1871, *Geophys. Res. Lett.*, *38*, L14703, doi:10.1029/2011GL047995.
Fagherazzi, S., L. Carniello, L. D'Alpaos, and A. Defina (2006), Critical bifurcation of shallow microtidal landforms in tidal flats and salt marshes, *Proc. Natl. Acad. Sci. U.S.A.*, *103*(22), 8337–8341.
Fagherazzi, S., et al. (2012), Numerical models of salt marsh evolution: Ecological, geomorphic, and climatic factors, *Rev. Geophys.*, *50*, RG1002, doi:10.1029/2011RG000359.
Fortin, M.-J., and M. R. T. Dale (2005), *Spatial Analysis: A Guide for Ecologists*, Cambridge Univ. Press, Cambridge, U. K.
Friedrichs, C. T. (2011), 3.06—Tidal flat morphodynamics: A synthesis, in *Treatise on Estuarine and Coastal Science*, edited by E. Wolanski and D. McLusky, pp. 137–170, Academic Press, Waltham.
Friedrichs, C. T., and D. G. Aubrey (1996), Uniform bottom shear stress and equilibrium hyposometry of intertidal flats, in *Coastal and Estuarine Studies*, vol. 50, edited by C. Pattiaratchi, pp. 405–429, AGU, Washington, D. C.
Friess, D. A., K. W. Krauss, E. M. Horstman, T. Balke, T. J. Bouma, D. Galli, and E. L. Webb (2012), Are all intertidal wetlands naturally created equal? Bottlenecks, thresholds and knowledge gaps to mangrove and saltmarsh ecosystems, *Biol. Rev.*, *87*(2), 346–366.
Green, M. O., and G. Coco (2007), Sediment transport on an estuarine intertidal flat: Measurements and conceptual model of waves, rainfall and exchanges with a tidal creek, *Estuarine Coastal Shelf Sci.*, *72*(4), 553–569.
Green, M. O., and G. Coco (2014), Review of wave-driven sediment resuspension and transport in estuaries, *Rev. Geophys.*, *52*, 77–117, doi:10.1002/2013RG000437.
Hasselmann, K., et al. (1973), *Measurements of Wind-Wave Growth and Swell Decay During the Joint North Sea Wave Project (JONSWAP)*, Deutches Hydrographisches Institut, Hamburg.
Hu, Z., T. Suzuki, T. Zitman, W. Uittewaal, and M. Stive (2014), Laboratory study on wave dissipation by vegetation in combined current-wave flow, *Coast. Eng.*, *88*, 131–142, doi:10.1016/j.coastaleng.2014.02.009.
Infantes, E., A. Orfila, T. J. Bouma, G. Simarro, and J. Terrados (2011), *Posidonia oceanica* and *Cymodocea nodosa* seedling tolerance to wave exposure, *Limnol. Oceanogr.*, *56*(6), 2223–2232, doi:10.4319/lo.2011.56.6.2223.
Johnson, J. B., and K. S. Omland (2004), Model selection in ecology and evolution, *Trends Ecol. Evol.*, *19*(2), 101–108, doi:10.1016/j.tree.2003.10.013.
Kirwan, M. L., and G. R. Guntenspergen (2012), Feedbacks between inundation, root production, and shoot growth in a rapidly submerging brackish marsh, *J. Ecol.*, *100*(3), 764–770, doi:10.1111/j.1365-2745.2012.01957.x.
Kirwan, M. L., and J. P. Megonigal (2013), Tidal wetland stability in the face of human impacts and sea-level rise, *Nature*, *504*(7478), 53–60, doi:10.1038/nature12856.
Kirwan, M. L., G. R. Guntenspergen, A. D'Alpaos, J. T. Morris, S. M. Mudd, and S. Temmerman (2010), Limits on the adaptability of coastal marshes to rising sea level, *Geophys. Res. Lett.*, *37*, L23401, doi:10.1029/2010GL045489.
Le Hir, P., W. Roberts, O. Cazaillet, M. Christie, P. Bassoullet, and C. Bacher (2000), Characterization of intertidal flat hydrodynamics, *Cont. Shelf Res.*, *20*(12–13), 1433–1459.
Marani, M., A. D'Alpaos, S. Lanzoni, L. Carniello, and A. Rinaldo (2007), Biologically-controlled multiple equilibria of tidal landforms and the fate of the Venice lagoon, *Geophys. Res. Lett.*, *34*, L11402, doi:10.1029/2007GL030178.
Mariotti, G., and S. Fagherazzi (2010), A numerical model for the coupled long-term evolution of salt marshes and tidal flats, *J. Geophys. Res.*, *115*, F01004, doi:10.1029/2009JF001326.
Mariotti, G., and S. Fagherazzi (2013), Wind waves on a mudflat: The influence of fetch and depth on bed shear stresses, *Cont. Shelf Res.*, *60*, S99–S110, doi:10.1016/j.csr.2012.03.001.
McKee, K. L., and W. H. Patrick (1988), The relationship of smooth cordgrass (*Spartina alterniflora*) to tidal datums: A review, *Estuaries*, *11*(3), 143–151, doi:10.1007/BF02689778.
Morris, J. T., P. V. Sundareshwar, C. T. Nietch, B. Kjerfve, and D. R. Cahoon (2002), Responses of coastal wetlands to rising sea level, *Ecology*, *83*(10), 2869–2877.
Mudd, S. M., S. M. Howell, and J. T. Morris (2009), Impact of dynamic feedbacks between sedimentation, sea-level rise, and biomass production on near-surface marsh stratigraphy and carbon accumulation, *Estuarine Coastal Shelf Sci.*, *82*(3), 377–389, doi:10.1016/j.ecss.2009.01.028.
Pawlowicz, R., B. Beardsley, and S. Lentz (2002), Classical tidal harmonic analysis including error estimates in MATLAB using T_TIDE, *Comput. Geosci.*, *28*(8), 929–937, doi:10.1016/S0098-3004(02)00013-4.
Reed, D. J. (1995), The response of coastal marshes to sea-level rise: Survival or submergence?, *Earth Surf. Processes Landforms*, *20*(1), 39–48.

Richardson, A. D., B. H. Braswell, D. Y. Hollinger, J. P. Jenkins, and S. V. Ollinger (2009), Near-surface remote sensing of spatial and temporal variation in canopy phenology, *Ecol. Appl.*, *19*(6), 1417–1428, doi:10.1890/08-2022.1.

Roberts, W., P. Le Hir, and R. J. S. Whitehouse (2000), Investigation using simple mathematical models of the effect of tidal currents and waves on the profile shape of intertidal mudflats, *Cont. Shelf Res.*, *20*(10–11), 1079–1097.

Saintilan, N., N. C. Wilson, K. Rogers, A. Rajkaran, and K. W. Krauss (2014), Mangrove expansion and salt marsh decline at mangrove poleward limits, *Glob. Change Biol.*, *20*(1), 147–157, doi:10.1111/gcb.12341.

Schwarz, C., T. Ysebaert, Z. Zhu, L. Zhang, T. J. Bouma, and P. M. J. Herman (2011), Abiotic factors governing the establishment and expansion of two salt marsh plants in the Yangtze Estuary, China, *Wetlands*, *31*(6), 1011–1021, doi:10.1007/s13157-011-0212-5.

Soulsby, R. (1997), *Dynamics of Marine Sands a Manual for Practical Applications*, Telford, London.

Spencer, K. L., and G. L. Harvey (2012), Understanding system disturbance and ecosystem services in restored saltmarshes: Integrating physical and biogeochemical processes, *Estuarine Coastal Shelf Sci.*, *106*, 23–32, doi:10.1016/j.ecss.2012.04.020.

Temmerman, S., T. J. Bouma, J. Van de Koppel, D. Van der Wal, M. B. De Vries, and P. M. J. Herman (2007), Vegetation causes channel erosion in a tidal landscape, *Geology*, *35*(7), 631–634.

Temmerman, S., P. Meire, T. J. Bouma, P. M. J. Herman, T. Ysebaert, and H. J. De Vriend (2013), Ecosystem-based coastal defence in the face of global change, *Nature*, *504*(7478), 79–83, doi:10.1038/nature12859.

Tucker, M. J., and E. G. Pitt (2001), *Waves in Ocean Engineering*, 1st ed., Elsevier Science, Oxford, U. K.

Van de Koppel, J., D. van der Wal, J. P. Bakker, and P. M. Herman (2005), Self-organization and vegetation collapse in salt marsh ecosystems, *Am. Nat.*, *165*(1), E1–E12.

Van der Wal, D., A. Wielemaker-Van den Dool, and P. M. J. Herman (2008), Spatial patterns, rates and mechanisms of saltmarsh cycles (Westerschelde, The Netherlands), *Estuarine Coastal Shelf Sci.*, *76*(2), 357–368.

Van Rijn, L. C. (2007), Unified view of sediment transport by currents and waves. I: Initiation of motion, bed roughness, and bed-load transport, *J. Hydraul. Eng.*, *133*(6), 649–667, doi:10.1061/(ASCE)0733-9429(2007)133:6(649).

Viles, H. A., L. A. Naylor, N. E. A. Carter, and D. Chaput (2008), Biogeomorphological disturbance regimes: Progress in linking ecological and geomorphological systems, *Earth Surf. Processes Landforms*, *33*(9), 1419–1435, doi:10.1002/esp.1717.

Wang, C., and S. Temmerman (2013), Does bio-geomorphic feedback lead to abrupt shifts between alternative landscape states? An empirical study on intertidal flats and marshes, *J. Geophys. Res. Earth Surf.*, *118*, 229–240, doi:10.1002/jgrf.20027.

Winterwerp, J. C., P. L. A. Erftemeijer, N. Suryadiputra, P. Van Eijk, and L. Zhang (2013), Defining eco-morphodynamic requirements for rehabilitating eroding mangrove-mud coasts, *Wetlands*, *33*(3), 515–526, doi:10.1007/s13157-013-0409-x.

Zhu, Z., T. J. Bouma, T. Ysebaert, L. Zhang, and P. M. J. Herman (2014), Seed arrival and persistence at the tidal mudflat: Identifying key processes for pioneer seedling establishment in salt marshes, *Mar. Ecol. Prog. Ser.*, *513*, 97–109, doi:10.3354/meps10920.